Macromolecules

ARTICLE

pubs.acs.org/Macromolecules

Effect of Lithium Polysulfides on the Morphology of Block Copolymer Electrolytes

Alexander A. Teran[†,§] and Nitash P. Balsara[*,†,‡,§]

[†]Environmental Energy Technologies Division, Lawrence Berkeley National Laboratory, Berkeley, California, 94720, United States

[‡]Materials Sciences Division, Lawrence Berkeley National Laboratory, Berkeley, California, 94720, United States

[§]Department of Chemical and Biomolecular Engineering, University of California, Berkeley, California, 94720, United States

Supporting Information

ABSTRACT:

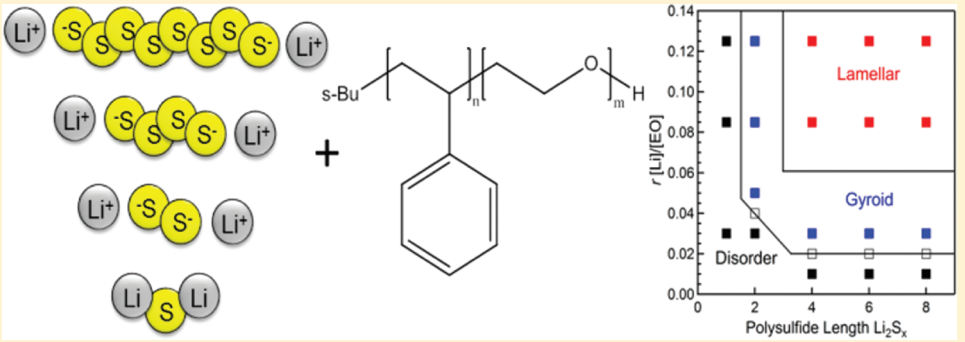

Lithium polysulfides (Li_2S_x, $1 \leq x \leq 8$) are produced during the discharge of lithium−sulfur batteries. Lithium−sulfur batteries are of interest due to their high energy density. The morphology of mixtures of polystyrene-*b*-poly(ethylene oxide) (SEO) copolymers and lithium polysulfides were studied using a combination of X-ray diffraction, small-angle X-ray scattering, differential scanning calorimetry, and ultraviolet−visible spectroscopy. This study is motivated by the possibility of using block copolymers as electrolytes in lithium−sulfur cells. The phase behavior of SEO/Li_2S_x mixtures were found to differ fundamentally from mixtures of SEO and other lithium salts. The morphology of certain SEO/Li_2S_x mixtures obtained below the melting temperature of the poly(ethylene oxide) block has not been previously observed in block copolymer/salt mixtures.

INTRODUCTION

Lithium−sulfur rechargeable cells are attractive because they offer a theoretical specific energy of 2600 Wh/kg, which is only a factor of 5 less than that of gasoline.[1,2] In contrast to cobalt- and nickel-based intercalation compounds used in the cathodes of conventional lithium-ion batteries, sulfur is inexpensive, nontoxic and abundant. The energy produced during discharge of the lithium−sulfur cell is due to a series of redox reactions involving Li^+ ions that diffuse from the anode to react with sulfur in the cathode. Elemental sulfur (S_8) is reduced through the following series of stepwise redox reactions

$$S_8 + 2Li^+ + 2e^- \rightarrow Li_2S_8$$

$$Li_2S_8 + 2Li^+ + 2e^- \rightarrow 2Li_2S_4$$

$$Li_2S_4 + 2Li^+ + 2e^- \rightarrow 2Li_2S_2$$

$$Li_2S_2 + 2Li^+ + 2e^- \rightarrow 2Li_2S_{(S)}$$

forming lithium polysulfide intermediates (Li_2S_x, $2 \leq x \leq 8$) with progressively shorter linear sulfur chains until the final reduction product lithium sulfide (Li_2S) is formed. The overall reaction can be represented $S_8 + 16Li^+ + 16e^- \rightarrow 8Li_2S$.

Despite its obvious advantages, lithium−sulfur chemistry has had limited commercial success due to significant challenges at both electrodes.[3,4] At the anode, lithium metal is reactive and prone to dendrite formation upon cycling, resulting in battery failure. Sulfur cathodes suffer from poor utilization of active material and rapid capacity fade upon cycling. The shortcomings of the sulfur electrode arise from the complexity of the species involved in the chemical reactions given above. The reactant and product of the overall reaction are insoluble and electronically insulating. Thus, in principle, the reaction can only be reversibly driven to completion if the reactants and products are confined within nanoscale electronically and ionically conducting channels. Additional complexity arises due to the solubility of the polysulfide intermediates ($2 \leq x \leq 8$) in organic electrolytes. The dissolution of these species into the electrolyte results in irreversible loss of active material from the cathode. To make

Received: September 14, 2011
Revised: October 26, 2011
Published: November 10, 2011

matters worse, these species can then be reduced at the anode, resulting in either the formation of a parasitic polysulfide shuttle between the electrodes,[5] or reduction at the cathode surface leading to uncontrolled precipitation.[6] In an important publication, the Nazar group showed that nanostructuring of the active sulfur particles in the electrode dramatically reduces irreversible capacity loss.[7] A logical question to ask is whether the performance of lithium−sulfur batteries can be improved by using a nanostructured electrolyte.

Previous work in our group has successfully shown that nanostructured block copolymer electrolytes, specifically polystyrene-*b*-poly(ethylene oxide) (SEO) doped with lithium bis(trifluoromethanesulfone)imide (LiTFSI), have high ionic conductivity at elevated temperature and sufficiently high modulus to prevent the formation of dendrites.[8] Additionally, the system has been shown to form a stable interface with lithium metal anodes as well as maintain intimate contact upon cycling.[9] Having already satisfied concerns pertaining to the lithium metal anode, we have begun to study the viability of this electrolyte against the sulfur cathode. An ideal electrolyte for a sulfur cathode would not allow the dissolution nor diffusion of the polysulfides out of the electrode. It is thus important to study the thermodynamic interactions between the lithium polysulfides and SEO block copolymers.

The present paper on the morphology of mixtures of polysulfides and SEO block copolymers may be considered an extension of previous studies on SEO/salt mixtures.[10−13] A major difference is that the polysulfide anions are divalent in contrast to all of the previous studies on SEO/salt mixtures, which are restricted to monovalent counterions. It is also known that polysulfide species undergo spontaneous reversible reactions such as

$$2Li_2S_6 \leftrightarrow Li_2S_4 + Li_2S_8$$

The equilibrium constants of the reactions depend on the medium. Thus, when we add a polysulfide to an SEO copolymer, it may transform to give a variety of other polysulfides. For example Li_2S_6 can transform into equal concentrations of Li_2S_4 and Li_2S_8.

The main purpose of this paper is to describe the phase behavior of SEO/Li_2S_x mixtures. The results presented here are qualitatively different from all previous studies of block copolymer/salt mixtures.

EXPERIMENTAL SECTION

Materials. The SEO copolymers in this study were synthesized via sequential anionic polymerization using methods described in refs 14 and 15. The polystyrene (PS) block was synthesized first using *sec*-butyllithium as the initiator. The poly(ethylene oxide) (PEO) block was then synthesized using P4 *tert*-butylphosphazene as a catalyst and terminated using methanol. The copolymers were purified by three rounds of precipitation in hexanes and subsequent dissolution in benzene. They were then passed three times through a column of neutral alumina and 0.2 μm cellulose filters. The copolymers were freeze-dried from benzene in a Millrock LD85 lyophilizer. The molecular weight and polydispersity index (PDI) of the PS blocks were obtained from aliquots of PS taken before the PEO chains were grown by gel permeation chromatography (GPC) using a tetrahydrofuran- (THF-) based Viscotek OmniSEC separations module and triple-detector system calibrated using PS standards. The volume fractions of each block and the molecular weight of the PEO blocks were determined using ^{1}H nuclear magnetic resonance (NMR) spectroscopy. The PDIs of the final SEO copolymers, $PDI_{polymer}$, were determined from a dimethylformamide (DMF)-based Viscotek OmniSEC GPC calibrated with PS standards. The polymers used in this study, which we call SEO(*xx-yy*) where *xx* and *yy* are the molecular weights of the PS and PEO blocks in kg/mol respectively, are listed in Table 1. PEO homopolymer was obtained from Polymer Source, Inc. The $PDI_{polymer}$ and M_{PEO} of PEO(1.1) are given in Table 1 is the value provided by the supplier. The neat polymers are completely transparent and colorless.

Table 1. Characteristics of the Polymers Used in This Study

polymer	M_{PS} (kg/mol)	M_{PEO} (kg/mol)	ϕ_{PEO} PEO vol frac	$PDI_{polymer}$
PEO(1.1)	–	1.1	1	1.10
SEO(1.7−1.4)	1.7	1.4	0.44	1.05
SEO(4.9−5.5)	4.9	5.5	0.51	1.04

Sample Preparation. Lithium polysulfides (Li_2S_x) were synthesized by dissolving stoichiometric amounts of elemental sulfur (S_8) and lithium sulfide (Li_2S) in dimethyl sulfoxide (DMSO)[16] and stirred for several days at 90 °C. The sulfur and lithium sulfide were received under argon from Alfa Aesar, opened in the glovebox, and used as received. Our synthesis procedure sets the value of, x_{av}, the molar average length of the polysulfide anion assuming the reactants are completely consumed. Detailed spectroscopic and electrochemical studies of polysulfide/DMSO mixtures indicate that the solutions thus obtained are dominated by a single species.[17] For example, when $x_{av} = 6$, the solution is predominantly composed of Li_2S_6. Similar studies have not been conducted in SEO copolymers. It is thus conceivable, for example, that the $x_{av} = 6$ mixtures in the SEO copolymers actually contain equal concentrations of Li_2S_4 and Li_2S_8. We synthesized polysulfides with values of $x_{av} = 1$, 2, 4, 6, and 8. It should be noted that the lithium polysulfide intermediates ($2 \leq x_{av} \leq 8$) cannot be isolated as pure compounds.[18] For simplicity, we refer to lithium polysulfides as salts.

All polymers were dried at 100 °C under vacuum in a glovebox antechamber for at least 24 h, and then brought immediately into the glovebox. The polysulfide solutions were added to polymers dissolved in DMSO. The polymer/salt solutions were then dried at 90 °C for 3 days in an airtight desiccator on a vacuum line under dynamic vacuum. Removal of solvent was confirmed using ^{1}H NMR and retention of polysulfides in the sample was confirmed using neutron activation analysis (NAA) performed by Elemental Analysis, Inc. (Drying at higher temperatures resulted in significant evaporation of the polysulfide species.) For values of $x_{av} \geq 2$, the dried polymer/salt mixtures have a deep red/orange color while the $x_{av} = 1$ mixtures are brown.

LiTFSI salt, obtained from Novolyte, was transferred from its air-free packaging into a vial inside of a glovebox, and then dried at 120 °C under vacuum in a glovebox antechamber for 3 days. The LiTFSI containing samples were prepared by blending an SEO/benzene solution with the necessary amount of a 25 wt % solution of LiTFSI salt in THF. Benzene and THF were purified using an MBraun solvent purification system to remove water and other impurities.

The molar salt concentration in our copolymers is quantified by the molar ratio of lithium atoms to ethylene oxide moieties, *r*, which ranges from 0.005 to 0.125. The number of EO units is the copolymer is calculated from the molecular weight of the PEO block without correcting for the −OH end groups. Because of the hygroscopic nature of the salts, argon gloveboxes (Vacuum Atmospheres Company) with oxygen and water at subppm levels were used for all sample preparation.

Small-Angle X-ray Scattering (SAXS). The structure of the polymer/salt mixtures were determined by SAXS. Samples were prepared by pressing/melting the polymer into 1 mm thick aluminum spacers and annealing at 90 °C for at least 24 h. The samples were sealed

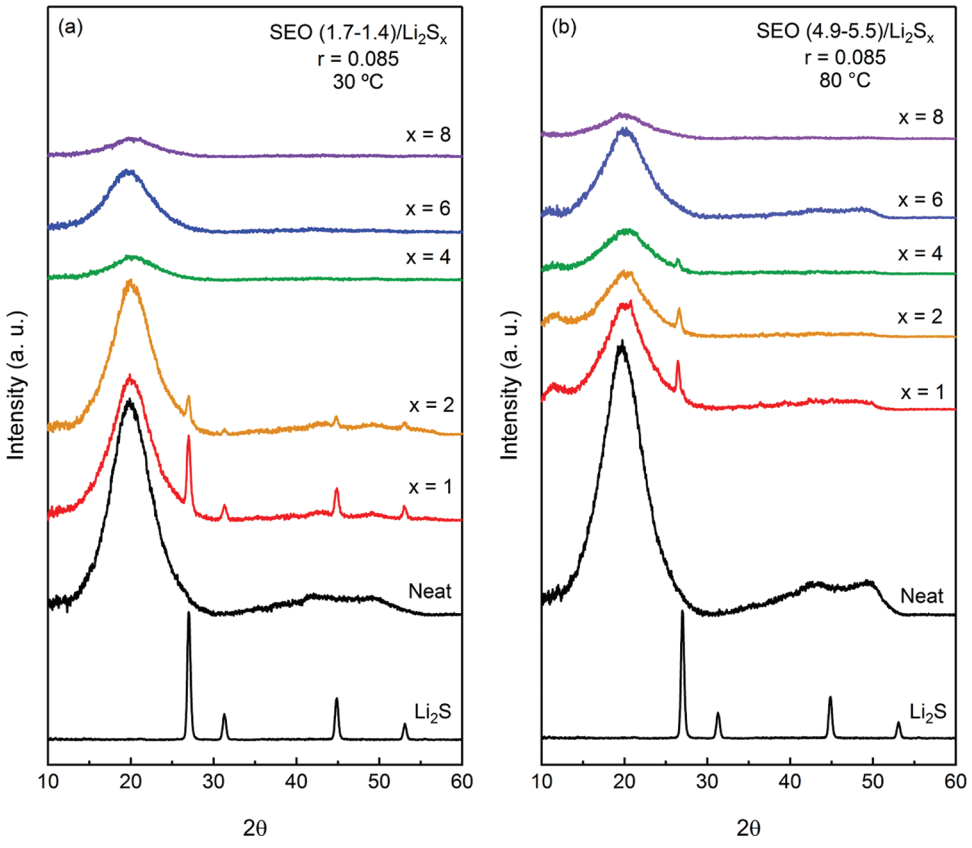

Figure 1. XRD intensity versus scattering angle, 2θ, of (a) SEO(1.7−1.4)/Li_2S_x at 30 °C and (b) SEO(4.9−5.5)/Li_2S_x at 80 °C with at a fixed concentration of $r = 0.085$, with $1 \leq x \leq 8$. Profiles are vertically offset for clarity. XRD of Li_2S is shown as a reference in both panels.

with Kapton windows in custom-designed airtight sample holders. Measurements were performed at beamline 7.3.3 at the Advanced Light Source (ALS) at Lawrence Berkeley National Laboratory. Samples were mounted in a custom-built heating stage and annealed at each temperature for 20 min before taking measurements. Silver behenate was used as a standard and scattering patterns were reduced using the Nika program for IGOR Pro available from Jan Ilavsky at Argonne National Laboratories. The azimuthally averaged scattering intensity, I, is reported as a function of the scattering vector q. The domain spacing, d, is defined as $d = 2\pi/q_{max}$, where q_{max} is the magnitude of the scattering vector q at the most intense peak. The value q^* is defined as the magnitude of the scattering vector associated with the {100} plane of a given morphology.

Differential Scanning Calorimetry (DSC). Samples were sealed in aluminum hermetic pans in the glovebox. DSC experiments were performed on a Thermal Advantage 2920 instrument. DSC scans consisted of three heating/cooling cycles and were conducted over the range −30 to +150 °C at a rate of 10 °C/min. The data presented is from the third heating run.

X-ray Diffraction (XRD). The same airtight sample holders used for SAXS were also used for XRD. The samples were run in transmission mode on a Bruker AXS D8 Discover GADDS XRD diffractometer operating at 40 kV and 20 mA and using Cu Kα radiation ($\lambda = 1.54178$ Å).

Ultraviolet−Visible Spectroscopy (UV−Vis). Samples were prepared by placing polymer in a double-sided Scotch tape "gasket", sandwiched between two quartz disks. The samples were then placed in custom-designed air-free aluminum sample holders. UV−vis measurements were made with a Varian Cary 50 instrument between 200 and 800 nm. The deep red/orange color of the mixtures necessitated the preparation of samples with extremely low salt concentrations ($r = 0.005$) and thicknesses no more than 100 μm in order to obtain absorbance values between approximately 0.3 and 1 before normalization for path length.

RESULTS AND DISCUSSION

We first focus on the X-ray diffraction profiles of the copolymers with the lithium polysulfides. Parts a and b of Figure 1 show the diffraction profiles for SEO(1.7−1.4)/Li_2S_x and SEO(4.9−5.5)/Li_2S_x, respectively, at a constant concentration of $r = 0.085$. For reference we also show diffraction profiles of the neat copolymers and pure lithium sulfide (Li_2S) in Figure 1. In the 2θ range shown, the Li_2S shows the expected {111}, {200}, {220}, {311} peaks, but the minor {222} peak at $2\theta = 56$ reported in the literature[19] was not observed. The XRD profiles of SEO(1.7−1.4)/Li_2S_x at 30 °C are shown in Figure 1a. The PEO block of pure SEO(1.7−1.4) does not crystallize, thus the amorphous PEO halo at 20° is the only feature present in the neat copolymer profile. For $x_{av} = 1$ and 2, diffraction peaks corresponding to those for Li_2S are visible, indicating the presence of Li_2S crystals in the mixtures. For $x_{av} = 4$, 6, and 8, there are no diffraction peaks visible, suggesting that the salts present are completely soluble in the polymer. The amorphous halo is significantly depressed for $x_{av} \geq 4$. Polysulfides with $2 \leq x_{av} \leq 8$ have not yet been isolated as pure compounds.[18] Thus, comparisons between the XRD data obtained from SEO/Li_2S_x mixtures with that of pure Li_2S_x are not possible for $x_{av} \geq 2$. The XRD data rule out the presence of Li_2S or S_8 in mixtures with $x_{av} > 4$, both of which have well-known powder diffraction patterns. No evidence of S_8 crystals are seen in any of the SEO/Li_2S_x mixtures.

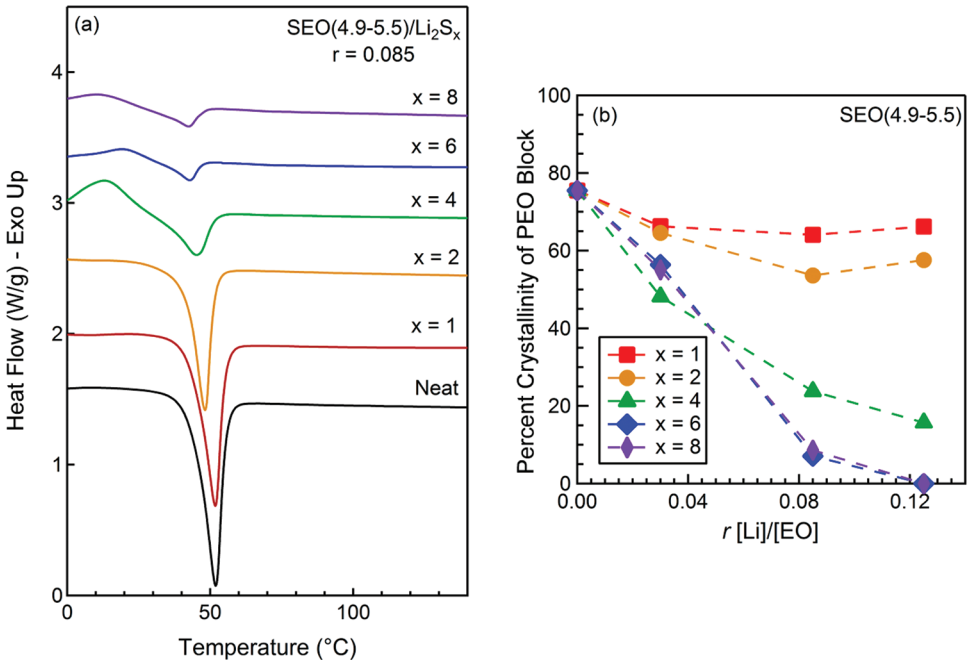

Figure 2. (a) DSC traces of SEO(4.9−5.5)/Li_2S_x at $r = 0.085$ and a heating rate of 10 °C/min. The third heating run is shown and profiles are vertically offset for clarity. (b) Effect of polysulfide length, x, and concentration, r, on the crystallinity of the PEO block for SEO(4.9−5.5)/ Li_2S_x samples.

The XRD profiles of SEO(4.9−5.5)/Li_2S_x at 80 °C (above the melting point of the PEO block) are shown in Figure 1b. The SEO(4.9−5.5)/Li_2S_x mixtures show the {111} peak of Li_2S for the x_{av} = 1, 2, and 4 samples. This suggests the presence of crystalline Li_2S at equilibrium with other species for values of x_{av} = 2 and 4. The trend of increasing solubility with increasing x_{av} seen in the copolymers is consistent with previous work on organic electrolytes[16] and homopolymers.[20,21]

Next we examine the thermal properties of the SEO copolymers with Li_2S_x. Figure 2a shows DSC scans of SEO(4.9−5.5)/Li_2S_x at a constant concentration of r = 0.085. The melting temperature, T_m, and the enthalpy of melting, ΔH_m, of the crystalline PEO decrease with increasing polysulfide length. The melting temperature decreases from 52 to 42 °C and ΔH_m decreases from 68.5 to 7.8 J/g as x_{av} is increased from 0 to 8. The exothermic peaks at low temperature for x_{av} = 4, 6, and 8 are the result of slow recrystallization of the PEO block. SEO(1.7−1.4)/Li_2S_x thermograms show no features (not shown). Figure 2b shows the effect of salt concentration on the crystallinity of the PEO block for each of the lithium polysulfides. For x_{av} = 1 and 2, the crystallinity appears to plateau as concentration increases while for x_{av} = 4, 6, and 8 crystallinity continues to decrease. For x_{av} = 6 and 8 at the highest concentration of r = 0.125, crystallinity is completely suppressed. The ether oxygens of the PEO backbone are able to coordinate lithium ions, causing the salt to preferentially segregate to that block, creating a PEO/Li_2S_x microphase. The coordination of the lithium ions disrupts the ability of the chain to crystallize. It is therefore expected that an increase in lithium ion concentration will result in a decrease in crystallinity. This is not seen for values of x_{av} = 1 and 2 indicating the lack of solubility of Li_2S_x in SEO(4.9−5.5). Similar conclusions can be made for SEO(1.7−1.4)/Li_2S_x based on the diffraction data above. It is worth noting that a fixed value of r, crystallinity decreases as polysulfide length increases. The DSC data support the conclusion that the solubility of the polysulfides increases with increasing x_{av}.

The phase behavior of SEO/Li_2S_x as a function of polysulfide length and salt concentration was obtained by SAXS. Parts a and b of Figure 3 show 1-D SAXS profiles for SEO(1.7−1.4)/ Li_2S_x and SEO(4.9−5.5)/Li_2S_x respectively at a constant concentration of r = 0.085 and at a temperature of 80 °C. Although both copolymers are disordered in their neat state at all temperatures, the addition of the polysulfides induces the stabilization of both lamellar (LAM) and gyroid (GYR) morphologies. In Figure 3a, SEO(1.7−1.4) in the neat state as well as with the addition of Li_2S shows no scattering peak, indicative of a disordered phase. As the value of x_{av} increases, there is increased segregation in the copolymers. The x_{av} = 2 sample shows a broad disordered peak. The peak appears to be a doublet which is typically not found in pure disordered block copolymers. The x_{av} = 4 and 6 samples show a distinct GYR morphology with sharp peaks at $q/q^* = \sqrt{6}$ and $\sqrt{8}$. It is possible that the disordered doublet at x_{av} = 2 are announcements of the ordered peaks seen at x_{av} = 4. The x_{av} = 8 sample has a LAM morphology with peaks at q/q^* = 1 and 2. In Figure 3b, SEO(4.9−5.5) shows a broad disordered peak for both the neat copolymer as well as upon the addition of Li_2S. The x_{av} = 2 sample shows a GYR morphology with distinct higher order peaks at $q/q^* = \sqrt{6}$, $\sqrt{8}$, $\sqrt{14}$, $\sqrt{16}$, $\sqrt{20}$, $\sqrt{22}$, $\sqrt{24}$, and $\sqrt{26}$, while the x_{av} = 4, 6, and 8 samples show LAM morphology with peaks at q/q^* = 1, 2, 3, and 4. In Figure 3 the molar concentration of lithium is held constant while the average length of the anion is increased. Increasing segregation with increasing anion radius is consistent with previous studies of SEO copolymers and monovalent salts.[10,13,22]

Several order−disorder transitions (ODTs) were observed in the SEO/Li_2S_x samples as temperature was increased. Figure 4 shows SAXS profiles for SEO(4.9−5.5)/Li_2S_8 at r = 0.02 at selected temperatures. The sample exhibits a GYR morphology from 60 to 120 °C. At 140 °C, the profile shows only the $q/q^* = 1$ and $\sqrt{3}$ peaks, indicating a hexagonally packed cylinder (CYL) phase. At 160 °C, the sample shows a single broad scattering peak corresponding to a disordered phase. The order−disorder

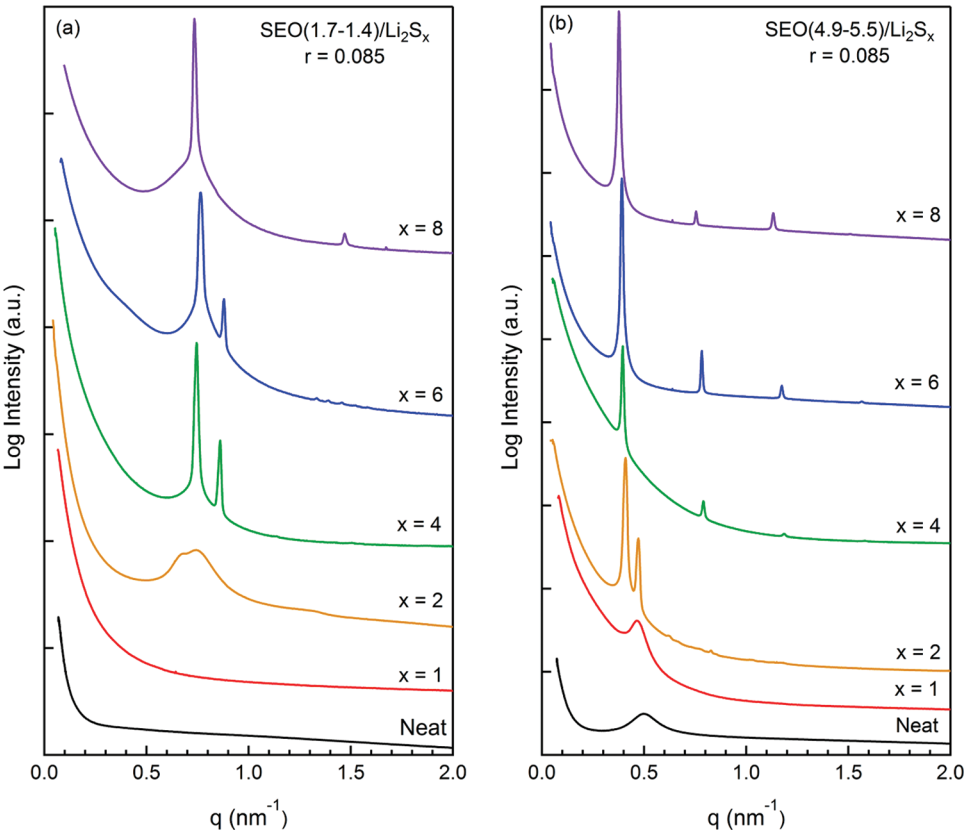

Figure 3. SAXS intensity versus scattering vector, q, for SEO/Li_2S_x at r = 0.085 at 80 °C. Profiles are vertically offset for clarity.

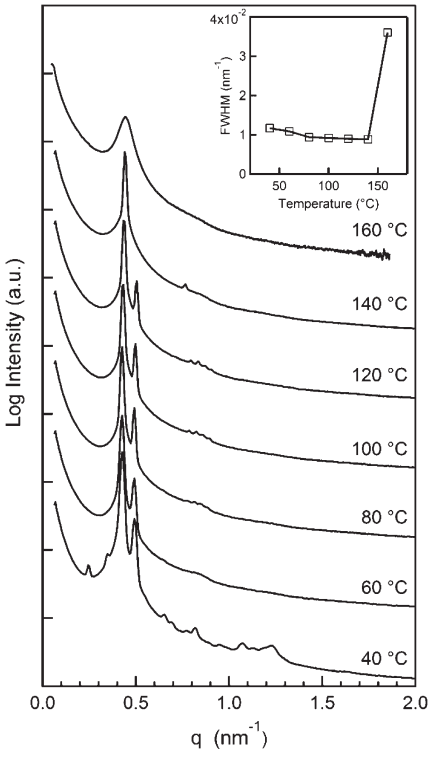

Figure 4. SAXS intensity versus scattering vector, q, for SEO(4.9−5.5)/Li_2S_8 at r = 0.02. Profiles are vertically offset for clarity. Inset shows fwhm of Gaussian fit to primary scattering peak as a function of temperature.

transition temperature (T_{ODT}) of this sample is determined to be 150 ± 10 °C by a sudden increase in the full width at half-maximum (fwhm) of the primary SAXS peak from 0.9×10^{-2} to 3.6×10^{-2} nm^{-1} as shown in the inset of Figure 4.

The SAXS data of SEO(4.9−5.5)/Li_2S_x samples at low salt concentrations and at temperatures below the melting point of PEO (e.g. 40 °C data in Figure 4) present an interesting puzzle. Figure 5a shows normalized SAXS profiles (I versus q/q_{max}) for several SEO(4.9−5.5)/Li_2S_x samples at 30 °C. These profiles are remarkable for several reasons. First, they show more than 17 higher order peaks corresponding to the GYR morphology, indicating the presence of considerable long-range order. Typically in semicrystalline block copolymers, samples below the melting point of the semicrystalline block exhibit poor long-range order due to interference of the crystals with microphase separation. This manifests itself in the form of broad peaks and absence of higher order peaks in SAXS profiles.[23] To our knowledge, SEO(4.9−5.5)/Li_2S_x is the only system that exhibits significantly enhanced long-range order when one of the blocks is crystallized (compare 40 and 60 °C data in Figure 4).

In addition to peaks corresponding to the GYR morphology (*Ia3d* space group), the SAXS profiles in Figure 5 contain three additional peaks at $q/q^* = \sqrt{2}$, $\sqrt{4}$, and $\sqrt{10}$. These peaks are normally forbidden for the *Ia3d* space group, but have been seen before in SAXS data from templated block copolymer nanocomposites.[24−28] The presence of the forbidden peaks in the block copolymer nanocomposites was first attributed to the presence of the plumber's nightmare morphology (*Im3m* space group).[28] In a subsequent paper,[24] some of the coauthors of ref 28

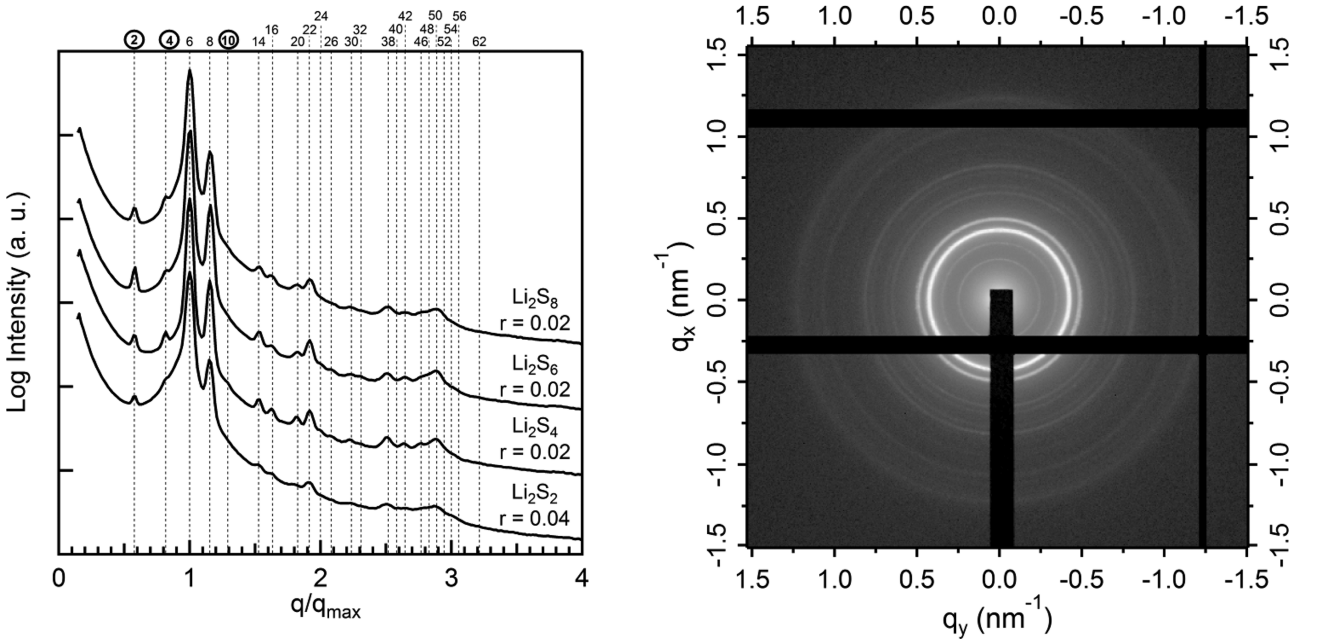

Figure 5. (a) SAXS intensity versus normalized scattering vector, q/q_{max} for SEO(4.9−5.5)/Li_2S_x at various values of x_{av} and r. Dotted vertical lines show all the expected Bragg reflections for the GYR morphology, as well as the three unexpected reflections at $h^2 + k^2 + l^2 = 2$, 4, and 10, shown circled on the top axis. Scattering profiles are vertically offset for clarity. (b) 2D SAXS intensity for SEO(4.9−5.5)/Li_2S_4 at $r = 0.02$.

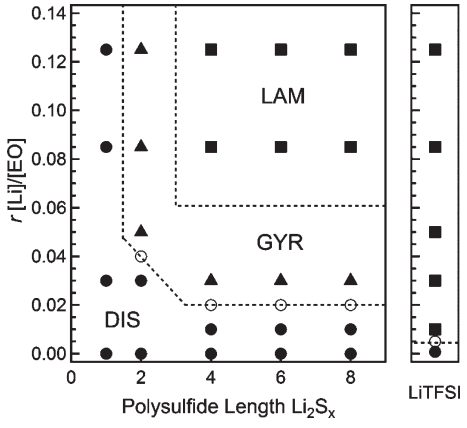

Figure 6. Phase diagram of SEO(4.9−5.5)/Li_2S_x and SEO(4.9−5.5)/LiTFSI. Full circles, triangles, and squares represent disordered, gyroid, and lamellar samples respectively. Open points bisected by the dotted phase boundary indicate a phase transition between the two neighboring phases was observed.

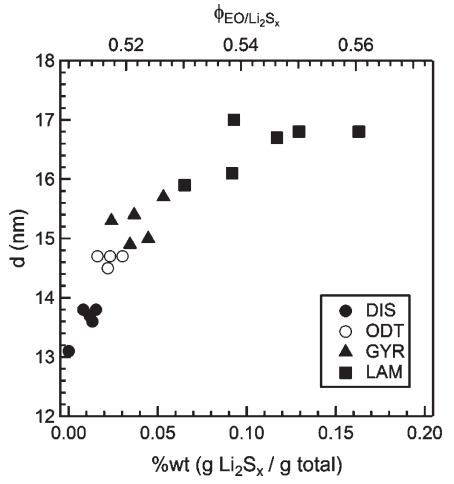

Figure 7. Domain spacing, d, versus weight percent salt, w, for SEO-(4.9−5.5)/Li_2S_x where $x \geq 2$. Estimated volume fraction of the PEO/Li_2S_x microphase is shown on top axis.

reanalyzed the data and attributed the presence of the forbidden peaks to a uniaxial deformation of the gyroid structure. The 2D scattering from such nanocomposite systems show sharp diffraction spots, whereas our samples exhibit isotropic rings such as those shown in Figure 5b.

In the Supporting Information, we compare the observed scattering peaks in Figure 5 with the expected SAXS peaks of all known cubic space groups. The GYR morphology is the one that is most consistent with the data. We thus tentatively conclude that crystalline SEO(4.9−5.5)/Li_2S_x mixtures form a "distorted" gyroid morphology and that the distortions arise due to interactions between Li_2S_x and crystalline PEO. Our attempts to substantiate our conclusion using transmission electron microscopy were unsuccessful. Difficulties arose due to the hygroscopic nature of the samples and the lack of instrumentation necessary to section and image samples without exposure to moisture. We hope to provide a definitive analysis of the samples discussed in Figure 5 in the near future when appropriate instrumentation is available.

The phase behavior observed for the SEO(4.9−5.5)/Li_2S_x samples is summarized in Figure 6 with salt concentration on the ordinate and polysulfide length on the abscissa. The diagram covers temperatures from 30 to 160 °C. The phase behavior of SEO(4.9−5.5)/LiTFSI is also shown in Figure 6. Each marker in Figure 6 represents a sample whose morphology was determined by SAXS. Markers bisected by a phase boundary indicate an

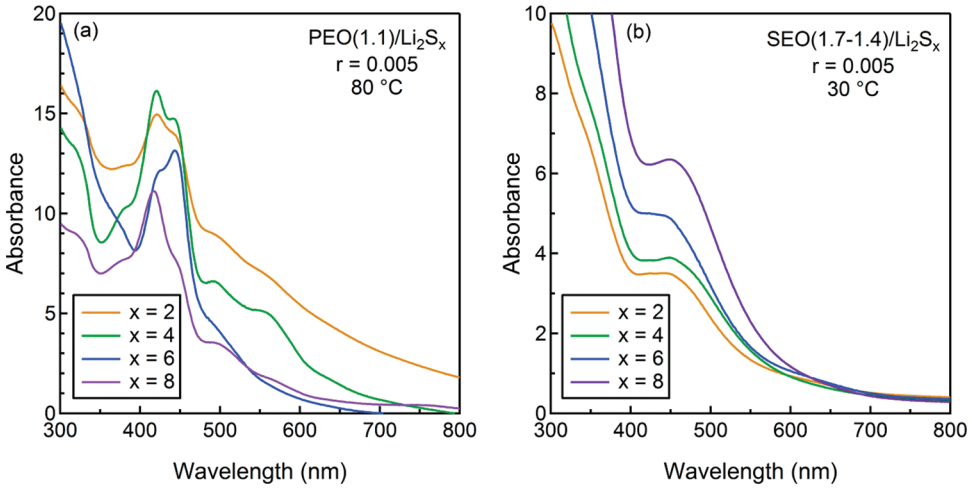

Figure 8. UV-vis spectra of dry mixtures of Li_2S_x at $r = 0.005$ in (a) PEO(1.1) at 80 °C and (b) SEO(1.7−1.4) at 30 °C. All spectra were normalized to 1 mm path length.

ODT was observed. In SEO(4.9−5.5)/Li_2S_x with $x_{av} = 4$, 6, and 8 at $r = 0.02$, the GYR-to-DIS transition is interrupted by a CYL phase. This was not observed in SEO(4.9−5.5)/Li_2S_2 at $r = 0.04$. We are not sure if this is due to the finite temperature steps used in this study. The symmetry of the phase diagram indicates that increasing the length of the anion by increasing the value of x_{av} has the same effect on the phase behavior of the copolymer as increasing the anion concentration, r. The disordered phase obtained at low values of x_{av} and r gives way to the GYR morphology at intermediate values of x_{av} and r. Further increase in x_{av} and r results in a GYR-to-LAM transition. An important observation is that the phase diagram of the block copolymer with the polysulfides and that of the block copolymer with LiTFSI are fundamentally different. Not only does SEO-(4.9−5.5) transition directly from DIS-to-LAM as salt is added, but the concentration of LiTFSI needed to induce ordering is lower by a factor of 5 on both a molar and weight basis. The phase behavior of SEO(1.7−1.4)/Li_2S_x and SEO(1.7−1.4)/LiTFSI showed a similar trend, though with an expected shift to higher salt concentrations due to molecular weight differences (not shown).

Figure 7 is a plot of domain spacing, d, versus the weight fraction of salt in the polymer, w, at a fixed temperature of 80 °C. The top axis shows the domain spacing versus the volume fraction of the PEO/Li_2S_x phase, ϕ_{EO/Li_2S_x}. The volume fraction calculations are estimates using the average density of lithium sulfide (1.66 g/cm^3) and sulfur (2.07 g/cm^3) as the density of the polysulfides and assuming perfect mixing of the salts in the PEO block. The different symbols in Figure 7 reflect different morphologies regardless of x_{av}. The collapse of all of the data onto a single curve and the clustering of similar morphologies in Figure 7 indicates that the morphology and domain spacing depends mainly on w, which reflects a particular combination of r and x_{av}.

The question of whether the PEO/Li_2S_x phase forms the network or the matrix of the GYR morphology is an interesting one. In diblock copolymer melts, increasing the volume fraction of the network-forming minority component results in a GYR-to-LAM transition.[29] Since increasing ϕ_{EO/Li_2S_x} results in a GYR-to-LAM transition (Figure 7), we conclude that the network must be composed of the PEO/Li_2S_x mixture. The GYR morphology is obtained when ϕ_{EO/Li_2S_x} is in the 0.51 to 0.53 range (Figure 7). In pure block copolymers, the gyroid network is formed by the minority phase at volume fractions of about 0.38. The presence of a salt-containing gyroid network that occupies more than 50% of the sample volume is further evidence of the unique and unprecedented thermodynamic properties that arise when lithium polysulfides are mixed with SEO copolymers. We have not included $x_{av} = 1$ samples in Figure 7 as it is clear from the calorimetry and X-ray scattering experiments that Li_2S is nominally immiscible in the SEO copolymers.

The value x_{av} is the average polysulfide length in the sample and we suspect that at any given value of x_{av} there exists an equilibrium between species with different values of x. Until this point we have provided no insight on the distribution of values of x present in the system. UV−vis spectroscopy has been used to distinguish the Li_2S_x speciation in organic solvents such as DMSO,[17,30−32] DMF,[33−37] THF,[2,16,30,38,39] dimethylacetamide,[40] liquid ammonia,[41,42] and acetonitrile.[43] Detailed spectroelectrochemical experiments are necessary for unambiguous determination of speciation.[17,32,34,41] These studies show that the distributions of species present depend crucially on the solvent. We have not yet embarked on such a study and thus we have not determined the species present in SEO block copolymers. Marmorstein et al.[20] used UV−vis spectroscopy to determine speciation in tetraethylene glycol, which may be regarded as an oligomeric PEO. However, the speciation model proposed in this study was not backed by the same rigorous analysis used in the studies involving other solvents. Figure 8a shows the UV−vis spectra of PEO(1.1)/Li_2S_x with $r = 0.005$ at 80 °C. We used low values of r because of the strong absorption of light in our samples. Even for very thin samples (100 μm thickness), light absorption was too high for the samples with higher values of r. The peaks of PEO(1.1)/Li_2S_x occur in the 400−500 nm region, the same region in which assignments for the species S_4^{2-}, S_6^{2-}, and S_8^{2-} have been made in DMSO.[17] We were, however, unable to make definitive assignments of species to specific peaks in the spectra. It should also be noted that our PEO spectra differ substantially from previous work by Marmorstein et al.[20] suggesting that factors such as polymer end group concentration may play an important role in speciation of Li_2S_x. Figure 8b shows the UV−vis spectra of SEO(1.7−1.4)/Li_2S_x with $r = 0.005$ at room temperature. The qualitative differences seen in

Figures 8a and 8b make it clear that solvation of Li_2S_x in homopolymer PEO and PEO contained within a block copolymer are very different. It is worth noting that SEO(1.7−1.4) used for the UV−vis experiment is disordered at $r = 0.005$. Previous studies indicate that even in the disordered state, SEO/salt mixtures are characterized by strong concentration fluctuations and the salt molecules are exclusively located within the PEO-rich fluctuating domains.[13] We thus expect the UV−vis spectra from the SEO(1.7−1.4)/Li_2S_x to reflect interactions between the salt and the PEO block. The qualitative similarity of the spectra of all of the samples in Figure 8b suggests that similar species are present in all of the samples. This implies that changing x_{av} as we have done in our experiments may primarily reflect the presence of different concentrations of the same S_x^{2-} anions. The presence of a dominant peak at 480 nm in all samples and the fact that this peak is most prominent in SEO(1.7−1.4)/Li_2S_2, suggests that the S_2^{2-} anion may be present in all samples. It is clear that further work is needed to fully characterize these mixtures. We note, however, that this is a nontrivial task as the experiments conducted on liquid systems are not easily done in the case of a solid electrolyte.

CONCLUSIONS

The phase behavior of mixtures of lithium polysulfide salts (Li_2S_x, $1 \leq x_{av} \leq 8$) and SEO diblock copolymers were studied using X-ray diffraction, differential scanning calorimetry, small-angle X-ray scattering, and UV−vis spectroscopy. The SEO copolymers were disordered in the neat state. The addition of the polysulfides resulted in disorder-to-order and order−order phase transitions. Increasing either the molar salt concentration, r, or anion size, x_{av}, resulted in increased segregation between the blocks. However, the morphology is primarily a function of the weight fraction of added salt, w. Increasing w from low to intermediate values results in a disorder-to-gyroid transition. At temperatures where the PEO block was crystalline, the SAXS profiles of the gyroid phase contains peaks that are normally forbidden. The SEO/Li_2S_x phase diagrams show fundamentally different morphologies than exhibited in other SEO/salt systems. Preliminary UV−vis experiments indicated that the solvation environment of the polysulfides in the SEO block copolymers is very different from that of PEO homopolymers. We have not determined the distribution of anion sizes at a given x_{av}. We hope to address this shortcoming in future publications. In spite of this, we feel that the present paper represents an important first step in understanding how species that are expected to form in a lithium−sulfur cell interact with a block copolymer electrolyte.

ASSOCIATED CONTENT

Supporting Information. Analysis of the SAXS data. This material is available free of charge via the Internet at http://pubs.acs.org/.

AUTHOR INFORMATION

Corresponding Author
*E-mail: nbalsara@berkeley.edu.

ACKNOWLEDGMENT

This work was supported by the Assistant Secretary for Energy Efficiency and Renewable Energy, Office of Vehicle Technologies of the U.S. Department of Energy under Contract No. DE-AC02-05CH11231, under the Batteries for Advanced Transportation Technologies (BATT) Program. A.A.T. was supported by a National Science Foundation Graduate Research Fellowship. XRD experiments were performed at the Molecular Foundry and SAXS experiments were performed at the ALS. Both are Lawrence Berkeley National Laboratory user facilities supported by the Director, Office of Science, Office of Basic Energy Sciences, of the U.S. Department of Energy, under Contract DE-AC02-05CH11231. The authors gratefully acknowledge Professor Rachel Segalman for use of equipment and Sunnie Mao and Sergey Yakovlev for their experimental help. The authors gratefully acknowledge insightful discussions with Dr. Hany Eitouni.

REFERENCES

(1) Rauh, R. D.; Abraham, K. M.; Pearson, G. F.; Surprenant, J. K.; Brummer, S. B. *J. Electrochem. Soc.* **1979**, *126* (4), 523–527.
(2) Yamin, H.; Gorenshtein, A.; Penciner, J.; Sternberg, Y.; Peled, E. *J. Electrochem. Soc.* **1988**, *135* (5), 1045–1048.
(3) Kolosnitsyn, V. S.; Karaseva, E. V. *Russ. J. Electrochem.* **2008**, *44* (5), 506–509.
(4) Akridge, J. R.; Mikhaylik, Y. V.; White, N. *Solid State Ionics* **2004**, *175* (1−4), 243–245.
(5) Mikhaylik, Y. V.; Akridge, J. R. *J. Electrochem. Soc.* **2004**, *151* (11), A1969–A1976.
(6) Cheon, S. E.; Ko, K. S.; Cho, J. H.; Kim, S. W.; Chin, E. Y.; Kim, H. T. *J. Electrochem. Soc.* **2003**, *150* (6), A796–A799.
(7) Ji, X. L.; Lee, K. T.; Nazar, L. F. *Nat. Mater.* **2009**, *8* (6), 500–506.
(8) Singh, M.; Odusanya, O.; Wilmes, G. M.; Eitouni, H. B.; Gomez, E. D.; Patel, A. J.; Chen, V. L.; Park, M. J.; Fragouli, P.; Iatrou, H.; Hadjichristidis, N.; Cookson, D.; Balsara, N. P. *Macromolecules* **2007**, *40* (13), 4578–4585.
(9) Stone, G. M.; Mullin, S. A.; Teran, A. A.; Hallinan, D. T.; Minor, A. M.; Hexemer, A.; Balsara, N. P. *J. Electrochem. Soc.* In review.
(10) Young, W. S.; Epps, T. H. *Macromolecules* **2009**, *42* (7), 2672–2678.
(11) Young, W. S.; Brigandi, P. J.; Epps, T. H. *Macromolecules* **2008**, *41* (17), 6276–6279.
(12) Wanakule, N. S.; Panday, A.; Mullin, S. A.; Gann, E.; Hexemer, A.; Balsara, N. P. *Macromolecules* **2009**, *42* (15), 5642–5651.
(13) Wanakule, N. S.; Virgili, J. M.; Teran, A. A.; Wang, Z.-G.; Balsara, N. P. *Macromolecules* **2010**, *43* (19), 8282–8289.
(14) Hadjichristidis, N.; Iatrou, H.; Pispas, S.; Pitsikalis, M. *J. Polym. Sci., Polym. Chem.* **2000**, *38* (18), 3211–3234.
(15) Quirk, R. P.; Kim, J.; Kausch, C.; Chun, M. S. *Polym. Int.* **1996**, *39* (1), 3–10.
(16) Rauh, R. D.; Shuker, F. S.; Marston, J. M.; Brummer, S. B. *J. Inorg. Nucl. Chem.* **1977**, *39* (10), 1761–1766.
(17) Kim, B. S.; Park, S. M. *J. Electrochem. Soc.* **1993**, *140* (1), 115–122.
(18) Pickering, T.; Tobolsky, A. *Sulfur in Organic and Inorganic Chemistry*; Marcel Dekker: New York, 1972; Vol. 3.
(19) Buehrer, W.; Altorfer, F.; Mesot, J.; Bill, H.; Carron, P.; Smith, H. G. *J. Phys.: Condens. Matter* **1991**, *3* (9), 1055–1064.
(20) Marmorstein, D. *Solid State Lithium/Sulfur Batteries for Electric Vehicles: Electrochemical and Spectroelectrochemical Investigations*; University of California: Berkeley, CA, 2002.
(21) Marmorstein, D.; Yu, T. H.; Striebel, K. A.; McLarnon, F. R.; Hou, J.; Cairns, E. J. *J. Power Sources* **2000**, *89* (2), 219–226.
(22) Wang, Z. G. *J. Phys. Chem. B* **2008**, *112* (50), 16205–16213.
(23) Ryan, A. J.; Hamley, I. W.; Bras, W.; Bates, F. S. *Macromolecules* **1995**, *28* (11), 3860–3868.
(24) Toombes, G. E. S.; Finnefrock, A. C.; Tate, M. W.; Ulrich, R.; Wiesner, U.; Gruner, S. M. *Macromolecules* **2007**, *40* (25), 8974–8982.

(25) Crossland, E. J. W.; Kamperman, M.; Nedelcu, M.; Ducati, C.; Wiesner, U.; Smilgies, D. M.; Toombes, G. E. S.; Hillmyer, M. A.; Ludwigs, S.; Steiner, U.; Snaith, H. J. *Nano Lett.* **2009**, *9* (8), 2807–2812.
(26) Stefik, M.; Mahajan, S.; Sai, H.; Epps, T. H.; Bates, F. S.; Gruner, S. M.; DiSalvo, F. J.; Wiesner, U. *Chem. Mater.* **2009**, *21* (22), 5466–5473.
(27) Urade, V. N.; Wei, T. C.; Tate, M. P.; Kowalski, J. D.; Hillhouse, H. W. *Chem. Mater.* **2007**, *19* (4), 768–777.
(28) Finnefrock, A. C.; Ulrich, R.; Toombes, G. E. S.; Gruner, S. M.; Wiesner, U. *J. Am. Chem. Soc.* **2003**, *125* (43), 13084–13093.
(29) Matsen, M. W.; Bates, F. S. *J. Polym. Sci., Part B: Polym. Phys.* **1997**, *35* (6), 945–952.
(30) Brummer, S. B.; Rauh, R. D.; Marston, J. M.; Shuker, F. S. *Low Temperature Lithium/Sulfur Secondary Battery*; Energy Research and Development Administration, US Department of Energy: Washington, DC, 1976; pp 1−57.
(31) Merritt, M. V.; Sawyer, D. T. *Inorg. Chem.* **1970**, *9* (2), 211.
(32) Martin, R. P.; Doub, W. H.; Roberts, J. L.; Sawyer, D. T. *Inorg. Chem.* **1973**, *12* (8), 1921–1925.
(33) Giggenbach, W. *J. Inorg. Nucl. Chem.* **1968**, *30* (12), 3189–&.
(34) Gaillard, F.; Levillain, E. *J. Electroanal. Chem.* **1995**, *398* (1−2), 77–87.
(35) Levillain, E.; Gaillard, F.; Lelieur, J. P. *J. Electroanal. Chem.* **1997**, *440* (1−2), 243–250.
(36) Levillain, E.; Gaillard, F.; Leghie, P.; Demortier, A.; Lelieur, J. P. *J. Electroanal. Chem.* **1997**, *420* (1−2), 167–177.
(37) Gaillard, F.; Levillain, E.; Lelieur, J. P. *J. Electroanal. Chem.* **1997**, *432* (1−2), 129–138.
(38) Yamin, H.; Penciner, J.; Gorenshtain, A.; Elam, M.; Peled, E. *J. Power Sources* **1985**, *14* (1−3), 129–134.
(39) Tobishima, S. I.; Yamamoto, H.; Matsuda, M. *Electrochim. Acta* **1997**, *42* (6), 1019–1029.
(40) Paris, J.; Plichon, V. *Electrochim. Acta* **1981**, *26* (12), 1823–1829.
(41) Levillain, E.; Gaillard, F.; Demortier, A.; Lelieur, J. P. *J. Electroanal. Chem.* **1996**, *405* (1−2), 85–94.
(42) Dubois, P.; Lelieur, J. P.; Lepoutre, G. *Inorg. Chem.* **1988**, *27* (1), 73–80.
(43) Fujinaga, T.; Kuwamoto, T.; Okazaki, S.; Hojo, M. *Bull. Chem. Soc. Jpn.* **1980**, *53* (10), 2851–2855.